Experimental Neurology **173,** 183–195 (2002)
doi:10.1006/exnr.2001.7754, available online at http://www.idealibrary.com on IDEAL®

# Time Course of the Development of Alzheimer-like Pathology in the Doubly Transgenic PS1+APP Mouse

Marcia N. Gordon, Leigh A. Holcomb,[1] Paul T. Jantzen, Giovanni DiCarlo, Donna Wilcock, Kristal W. Boyett, Karen Connor, Jason Melachrino, James P. O'Callaghan,* and Dave Morgan

*Alzheimer Research Laboratory, Department of Pharmacology, University of South Florida, Tampa, Florida 33612-4799; and *National Institute for Occupational Safety and Health/Center for Disease Control, MS 3014, Morgantown, West Virginia 26505-2888*

Received February 12, 2001; accepted June 18, 2001; published online August 24, 2001

**Doubly transgenic mice expressing both a mutated amyloid precursor protein and a mutated presenilin-1 protein accumulate A$\beta$ deposits as they age. The early A$\beta$ deposits were found to be primarily composed of fibrillar A$\beta$ and resembled compact amyloid plaques. As the mice aged, nonfibrillar A$\beta$ deposits increased in number and spread to regions not typically associated with amyloid plaques in Alzheimer's disease. The fibrillar, amyloid-containing deposits remained restricted to cortical and hippocampal structures and did not increase substantially beyond the 12-month time point. Even at early time points, the fibrillar deposits were associated with dystrophic neurites and activated astrocytes expressing elevated levels of glial fibrillary acidic protein. Microglia similarly demonstrated increased staining for complement receptor-3 in the vicinity of A$\beta$ deposits at early time points. However, when MHC-II staining was used to assess the degree of microglial activation, full activation was not detected until mice were 12 months or older. Overall, the regional pattern of A$\beta$ staining resembles that found in Alzheimer disease; however, a progression from diffuse A$\beta$ to more compact amyloid deposits is not observed in the mouse model. It is noted that the activation of microglia at 12 months is coincident with the apparent stabilization of fibrillar A$\beta$ deposits, raising the possibility that activated microglia might clear fibrillar A$\beta$ deposits at a rate similar to their rate of formation, thereby establishing a relatively steady-state level of amyloid-containing deposits.** 

## INTRODUCTION

Transgenic mouse models of Alzheimer disease are useful for understanding the mechanisms by which specific mutations might lead to the Alzheimer phenotype and to test possible therapeutics. Since the original description of amyloid precursor protein (APP) transgenic mice depositing fibrillar A$\beta$ (11), there have been a number of additional transgenic lines described, with varying degrees of the Alzheimer phenotype (19, 43, 34). Although presenilin-1 (PS1) transgenic mice do not themselves deposit A$\beta$ (3, 7, 9), the PS1 transgene potentiates the deposition of A$\beta$ in APP mice (6, 18).

Johnson-Wood *et al.* (24) quantified the deposition of A$\beta$ over the life span of the PDAPP mouse first described by Games *et al.* (11). While others have described some of the changes in these doubly transgenic mice (6, 16, 17, 29, 44), a detailed time course measuring diffuse and fibrillar A$\beta$ loads plus glial activation has not been performed. We report here the time course of A$\beta$ deposition and the activation of microglia in the doubly transgenic APP+PS1 mice. In a related paper, Jaffar *et al.* (22) detail the regional localization and other qualitative features of this model for Alzheimer research, focusing on 12-month-old animals.

## MATERIALS AND METHODS

*Materials.* Doubly transgenic mice for this study were originally obtained by crossing Tg2576 APP mice of Hsiao *et al.* (19) with line 5.1 PS1 mice of Duff *et al.* (9) as described by us previously (18). Mice were group-housed where possible, although occasional male mice had to be housed in isolation to avoid intermale aggression. Because the two transgenes segregate independently, offspring of four genotypes result: nontransgenic, PS1 transgenic, APP transgenic, and doubly transgenic APP+PS1. The vivarium was on a 12/12 L/D cycle and food and water were available *ad libitum*. Genotypes were confirmed by slot blots shortly after weaning and confirmed at necropsy.

Antisera/bodies used for these studies are detailed in Table 1. Total A$\beta$ antisera (A$\beta_{TOT}$) were from rabbits immunized with A$\beta$1-40 peptide as described previously (13). Competition ELISA studies with different A$\beta$ peptide fragments indicate that the main epitope is

[1] Present address: Texas A&M HSC, Department of Psychiatry & Behavioral Sciences, Research Office 151T, 1901 S. 1st St., Temple, TX 76504.



0014-4886/01 $35.00

**TABLE 1**

Antibodies Used for Immunostaining

| Antigen | Type | Source | Clone | Titer |
|---|---|---|---|---|
| $A\beta_{TOT}$ | Polyclonal | P. Gottschall | | 1:10,000 |
| A$\beta$42 | Polyclonal | QCB | | 0.5 $\mu$g/ml |
| A$\beta$40 | Polyclonal | QCB | | 0.5 $\mu$g/ml |
| GFAP | Polyclonal | Zymed | | 1:10,000 |
| Phosphorylated neurofilament | Monoclonal | Sternberger Monoclonals | SMI-312 | 1:100,000 |
| APP | Monoclonal | Boehringer | 22c11 | 1:1000 |
| Synaptophysin | Polyclonal | Dako | | 1:10,000 |
| Ubiquitin | Polyclonal | Dako | | 1:3000 |
| Perlecan | Polyclonal | B. Greenberg | | 1:30,000[a] |
| CR3, CD11, mac-1 | Monoclonal | Harlan/BioProducts Science | 5C6 | 1:10,000 |
| MHC-II | Polyclonal | BD Pharmingen | M5/114.15.2 | 1:10,000 |

[a] Even at 1:1000 concentration no plaque staining was visible.

within the first 16 residues of the peptide, and this antiserum recognizes all C-terminal variants of the A$\beta$ peptide. Selectivity for immunocytochemistry of $A\beta_{TOT}$, A$\beta$40, and A$\beta$42 antisera was confirmed by separate preabsorption experiments with A$\beta$1-40 and A$\beta$1-42 peptides. Antisera specific for A$\beta$ peptides ending at residue 40 (A$\beta$40) and A$\beta$ peptides ending at residue 42 (A$\beta$42) were obtained from Quality Controlled Biochemical (QCB; Hopkinton, MA). Thioflavin S and Congo red stains were obtained from Sigma.

*Tissue staining.* Mice ranging from 3 to 18 months of age (roughly 50) were anesthetized with pentobarbital (100 mg/kg ip) and perfused transcardially with 25 ml normal (0.9%) saline. The brains were rapidly removed and the left hemispheres were immersion fixed in freshly depolymerized 4% paraformaldehyde (buffered to pH 7.4 in potassium phosphate) for 24 h, then cryoprotected in a series of sucrose solutions. The right hemispheres were rapidly dissected on a cold stage into hippocampus + neocortex (amyloid containing) and basal forebrain + brain stem (non-amyloid containing) regions, frozen on dry ice, and stored at −70°C. Fixed, cryoprotected left hemispheres were frozen and sectioned in the horizontal plane at 25 $\mu$m using a sliding microtome and stored at 4°C in Dulbecco's phosphate-buffered saline for immunocytochemistry and histology. Immunocytochemistry was performed on floating sections as described in detail previously (14). It should be noted that for each antibody reaction, sections from mice of all ages were stained in the same antibody solution using multisample staining racks and trays. However, due to limited amounts of tissue, not all mice were stained by all methods (see figure captions for the sample size of each group).

Sections were incubated with the primary antibody 18 h at 4°C, then incubated in the biotinylated secondary antibody (120 min) followed by avidin–biotin–peroxidase complex using the Vectastain Elite kit. Peroxidase reactions consisted of 1.4 mM diaminobenzidine with 0.03% hydrogen peroxide in PBS for exactly 5 min. For markers of microglia and dystrophic neurites, 0.5% nickelous ammonium sulfate was included in the peroxidase reactions, rendering positive stain a dark blue color. This maximized differentiation of immunostaining from the Congo red counterstain (method described below). Nonspecific reaction product formation was negligible as assessed by omitting the primary antibody and comparing the staining in transgenic mice to nontransgenic animals. Each assay was balanced with respect to the experimental age groups.

Congo red and thioflavin S histology were carried out using sections mounted on slides and air dried for a minimum of 12 h, then rehydrated for approximately 30 s before staining. For Congo red, hydrated sections were incubated in an alkaline alcoholic saturated sodium chloride solution (2.5 mM NaOH in 80% ethanol, freshly prepared) for 20 min, then incubated in 0.2% Congo red in alkaline alcoholic saturated sodium chloride solution (freshly prepared and filtered) for 30 min. For thioflavin S, sections were stained for 15 min in a 1% solution and quickly rinsed with water. For both stains, sections were rinsed through three rapid changes of 100% ethanol, cleared through three changes of xylene, and then coverslipped with DPX (E.M. Sciences, Fort Washington, PA).

Sections for silver staining were collected in freshly prepared 4% paraformaldehyde and fixed for an additional week, before staining using the FD NeuroSilver kit as described by the manufacturer (FD Neuro Technologies, Ellicott City, MD).

*Glial fibrillary acidic protein (GFAP) ELISA.* GFAP was assayed according to the detergent-based "sandwich" ELISA of O'Callaghan (35), with minor modifications. Briefly, a rabbit polyclonal antibody to GFAP (Dako) was coated on the wells of Immulon-2 microtiter plates (Dynatech Laboratories, Chantilly, VA). After blocking nonspecific binding with nonfat dry milk, aliquots of the 1% SDS homogenates of brain

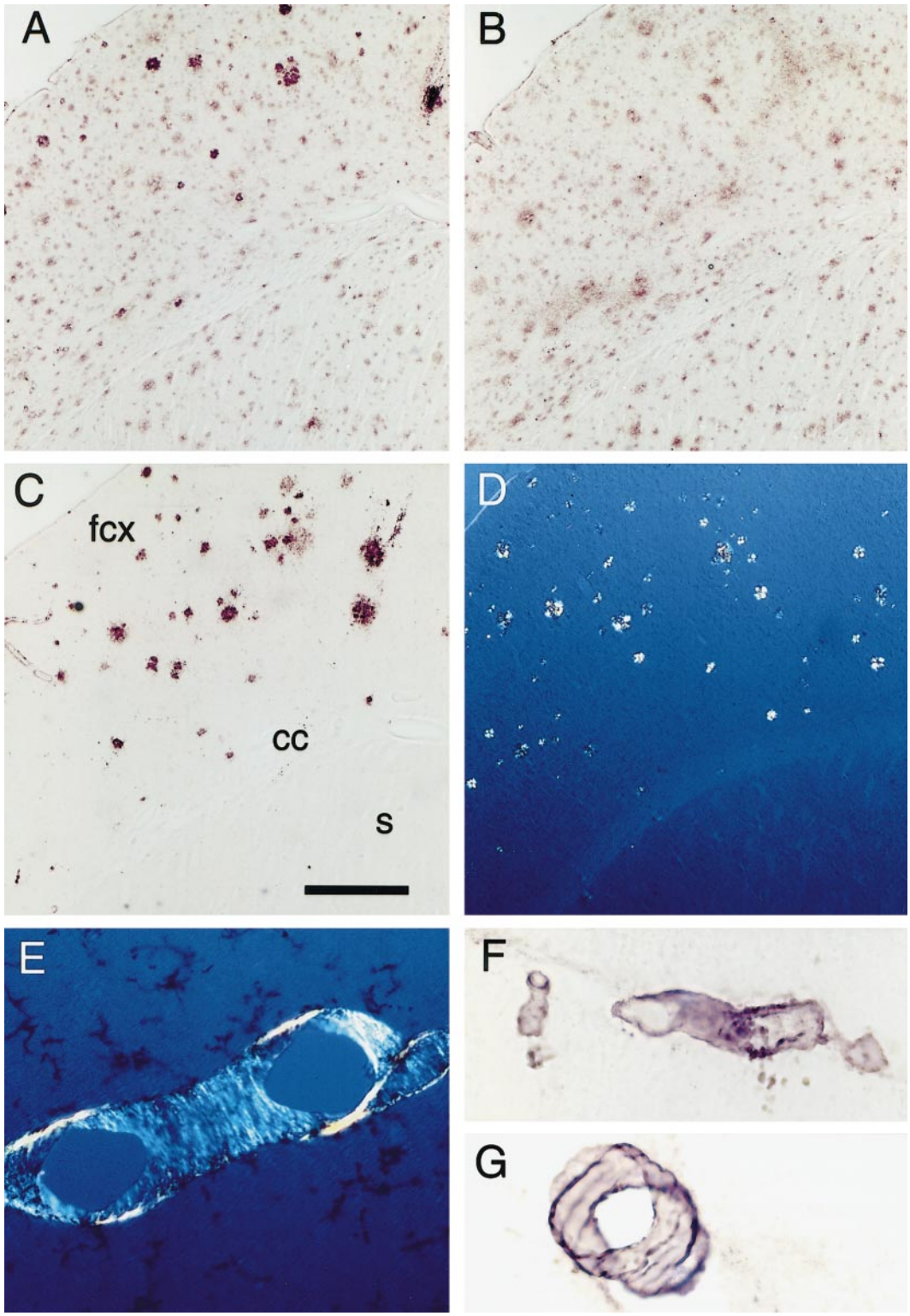


**FIG. 1.** Distribution of A$\beta$ variants in doubly transgenic mice. Anterior regions of a 15-month-old PS+APP transgenic mouse were immunostained for A$\beta_{TOT}$ (A), A$\beta$42 (B), and A$\beta$40 (C) for bright-field microscopy or stained with Congo red and viewed with cross-polarized illumination (D, E). The regions indicated as frontal cortex (fcx), corpus callosum (cc), and striatum (s) in C apply to (A–D). Vascular amyloid could also be detected with Congo red staining (E) and A$\beta$40 antisera (F, G). Scale bar, 250 $\mu$m in A–D and 25 $\mu$m in E–G.

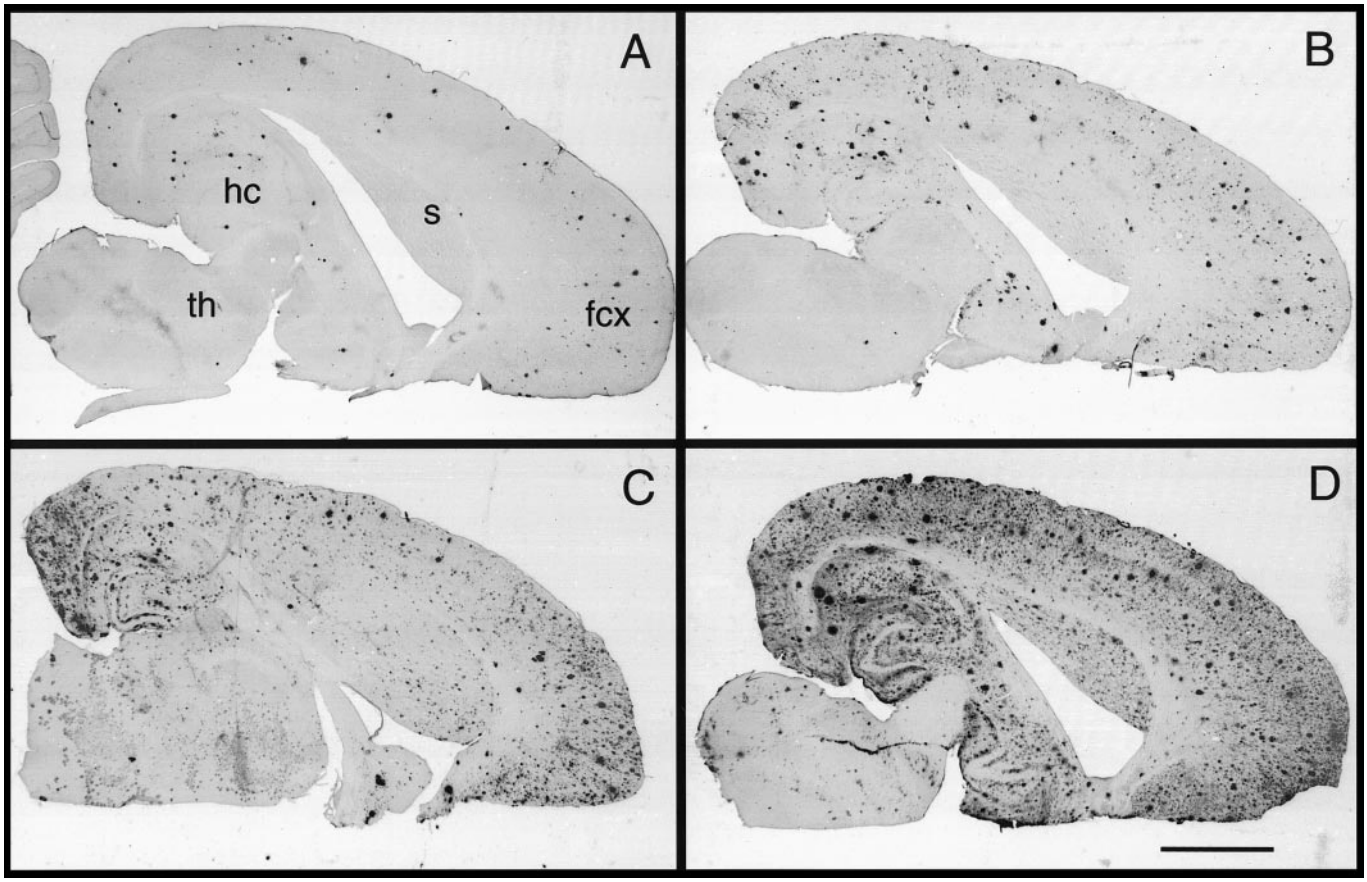


**FIG. 2.** Time course of $A\beta_{TOT}$ deposition in doubly transgenic mice. Horizontal sections were immunostained as described under Materials and Methods. Sections from mice at 6 (A), 9 (B), 12 (C), and 15 months (D) are compared. Scale bar, 1 mm. Abbreviations: fcx, frontal cortex; s, striatum; hc, hippocampus; th, thalamus.

tissue, prepared as described (35), were diluted in sample buffer and added to the wells of the plate. After appropriate blocking and washing steps, a mouse monoclonal antibody to GFAP (Chemicon) was added to sandwich GFAP between the two antibodies. In the original method (35) an alkaline phosphatase-linked antibody (Jackson ImmunoResearch Laboratories) directed against mouse IgG then was added. In the modification, the monoclonal antibody to GFAP was mixed with the alkaline phosphatase-linked secondary and they were added in a single step. Quantification of the colored reaction product was achieved by spectrometry at 405 nm using a microplate reader (UV Max running on a Soft Max program; Molecular Devices, Menlo Park, CA). Total protein concentration in the SDS homogenates was determined by the method of Smith *et al.* (40). Bovine serum albumin (Sigma) was used as the standard.

*Image analysis.* Immunocytochemistry or Congo red staining of tissue sections was quantified with an Oncor V150 color image analysis system. The software used hue, saturation, and intensity (HSI) to segment objects in the image field. Thresholds for object segmentation were established using a series of standard slides which have the extremes of intensity for the stain being measured. Thresholds in HSI space which accurately identify objects on all standard slides were established and these segmentation thresholds remained constant throughout the analysis session. A constant voltage power source was used to reduce fluctuations in microscope illumination or video camera sensitivity during each measurement session. Section-to-section variability in immunostaining intensity was minor owing to rigid fixation and staining protocols. The HSI segmentation parameters accurately identify positive staining on all sections. The operator was unaware of the experimental condition when measurements were taken. Staining in the frontal cortex and the hippocampus was quantified from horizontal sections from each mouse (ranging from 4 to 16 sections total for each mouse depending upon the antibody used), spaced between 2000 and 3600 $\mu$m ventral to bregma. The sections from each mouse were matched as closely as possible. To consistently identify the same field in each section, the measurement area was carefully positioned using the following criteria. The fron-

tal cortex measurement used an 80× field with one limit of the field of view resting on the superficial edge of the cortex and the other limit aligned with the midline of the section in the most anterior position possible. The measurement area was a rectangular video field of 850,000 $\mu m^2$ (0.85 $mm^2$) located within the center of that field of view. The measurement area was primarily of the middle 2/3 of the cortical mantle (i.e., generally not including cortical layers 1 or 6). Hippocampus used the standard boundaries of the fimbria anteriorly, ventricle medially, and corpus callosum laterally and posteriorly. "A$\beta$ load" was the percentage of area in the measurement field occupied by reaction product. Similarly, "Congo red staining" refers to the percentage of the area that is stained with Congo red. All values from a given mouse were averaged to represent the single value for that animal.

## RESULTS

Doubly transgenic PS1+APP mice deposited large amounts of A$\beta$ peptide in cerebral cortex (Fig. 1) and hippocampus (Fig. 2). In general, the distribution of immunostaining with an antiserum that is specific for the N-terminal portion of the A$\beta$ peptide ($A\beta_{TOT}$) was similar to that obtained with an antiserum specific for A$\beta$42, with both diffuse and compact deposits being labeled (Figs. 1A and 1B). One difference is that the $A\beta_{TOT}$ antiserum labeled compact deposits more intensely than the A$\beta$42 antiserum. Both antisera labeled deposits in the cerebral cortex, corpus callosum, and striatum in the anterior portion of horizontal sections as shown in Fig. 1.

In contrast, antiserum specific for A$\beta$40 labeled primarily the compact deposits (Fig. 1C) and some blood vessels (Figs. 1C, 1F, and 1G). The distribution of A$\beta$40 immunostaining paralleled that of Congo red staining (Fig. 1D). Congo red stained only the compact deposits and did not extend into the striatum, a feature shared with the A$\beta$40 antiserum (Fig. 1C and 1D). The deposits in blood vessels were also congophilic, indicating the presence of A$\beta$ fibrils at these sites (Fig. 1E).

By 6 months of age, all doubly transgenic mice had multiple deposits on all sections. The highest densities initially were in frontal and entorhinal cortices and hippocampus (Fig. 2A). At this age the thalamus and striatum were free of deposits. All A$\beta$ deposits were darkly stained and appeared compact (Fig. 2A) and most were also stained with A$\beta$40 and Congo red. At 9 months of age (Fig. 2B), the number of deposits increased, with some diffuse A$\beta$ present. At 12 (Fig. 2C) and 15 months of age (Fig. 2D), the density of deposits was further increased, with large amounts of diffuse A$\beta$ present. The granule and pyramidal cell layers of the hippocampus and the corpus callosum were negatively stained, as the A$\beta$ deposits were excluded from these laminae. Also more obvious after 12 months, A$\beta$ deposits increased in the striatum, thalamus, and brain stem (Figs. 2C and 2D). However, these were exclusively diffuse deposits and not labeled with A$\beta$40 antiserum or Congo red.

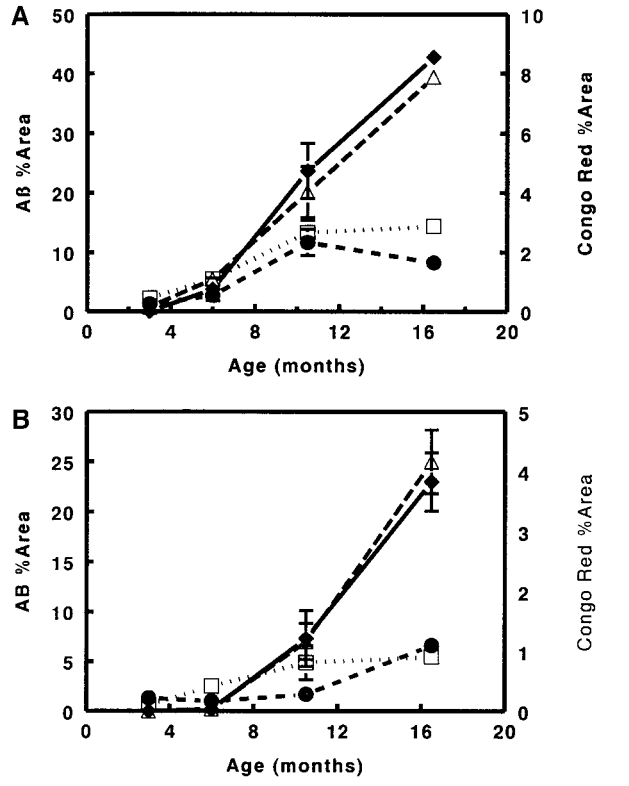


**FIG. 3.** Amyloid burden increases with age in frontal cortex and hippocampus. The amyloid burden was measured in frontal cortex (A) or hippocampus (B) as described under Materials and Methods. The areas stained positively with antiserum for $A\beta_{TOT}$ (open triangles), A$\beta$42 (solid diamonds), and A$\beta$40 (open squares) are plotted against the left axis. The area stained with Congo red (solid circles) is plotted against the right axis. The *n* for each group is 4 in the 3- and 6-month-old groups, 10 in the 10.5- (range 9–12 months) and 11 in the 16.5-month (range 15–18 months) age groups. Data presented are means ± SEM. In some cases the SEM is smaller than the size of the symbol and does not appear on the graph.

The image analysis results for the time course of A$\beta$ deposition are presented in Fig. 3. At 3 months, none of the mice had detectable immunostaining with any of the methods. In both frontal cortex (Fig. 3A) and hippocampus (Fig. 3B), all measures of A$\beta$ deposition tended to increase up to 9–12 months of age. After this time the amount of diffuse A$\beta$ as measured by $A\beta_{TOT}$ and A$\beta$42 immunostaining continued to increase, ultimately covering almost 50% of the cross-sectional area in the frontal cortex and 25% in the hippocampus. Conversely, the staining for compact material with A$\beta$40 and Congo red remained relatively stable from the 9–12 month time point to the 15–18 month time points. This stabilization was most apparent in the frontal cortex region we measured. In hippocampus,

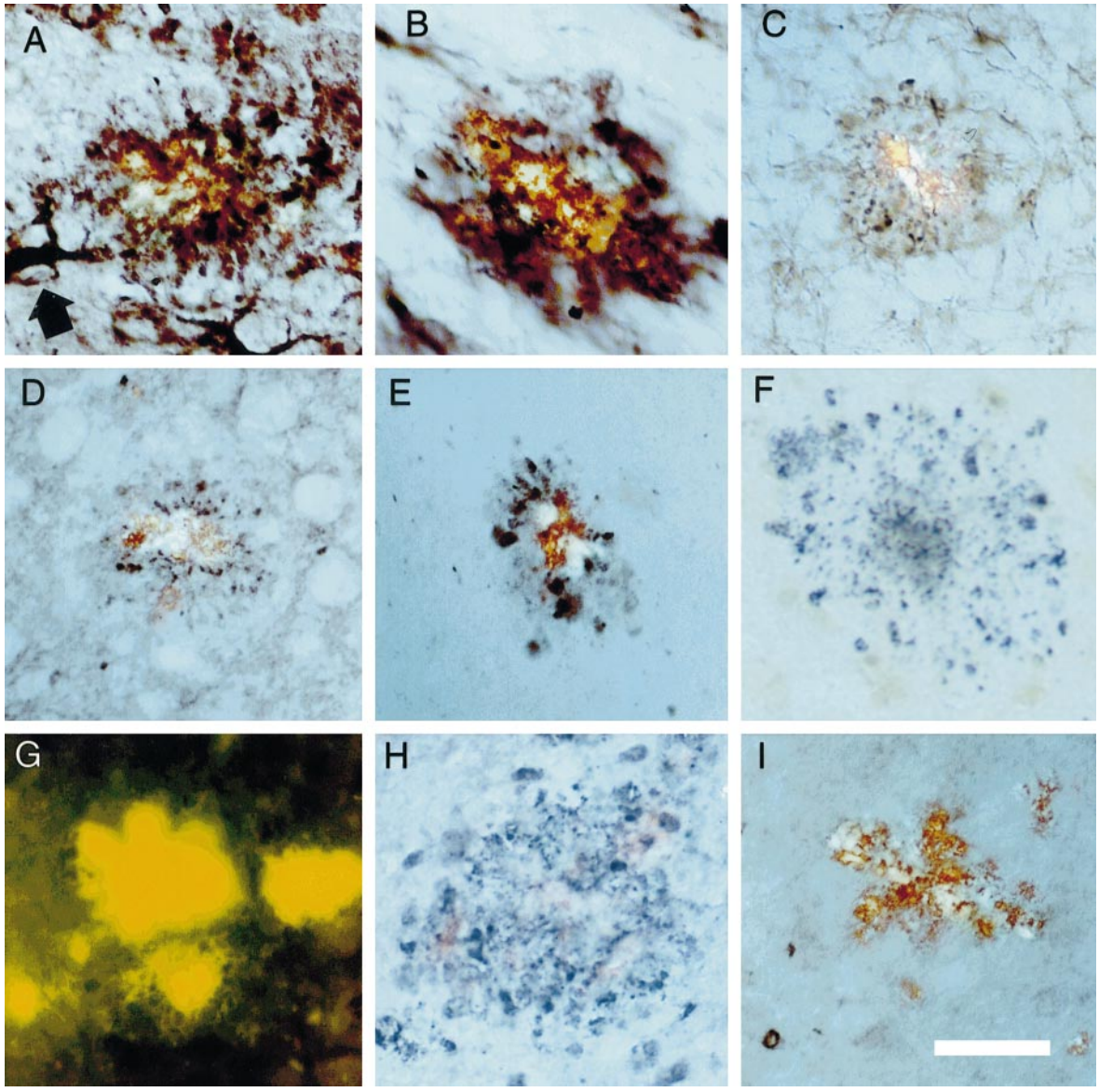


**FIG. 4.** Staining of dystrophic neurites in doubly transgenic mice. Neurites in the vicinity of amyloid deposits could be discerned in 6-month-old mice using antiserum to APP in both gray matter (A) and white matter (B), using anti-neurofilament antibody SMI-312 (C), using anti-synaptophysin antiserum in both gray matter (D) and white matter (E), using silver stain (F), or using ubiquitin staining (H). Plaques could also be visualized using thioflavin S fluorescence (G). However, antibody against the heparan sulfate proteoglycan perlecan was restricted to the vascular basement membrane and did not label neurites or deposits. Scale bar, 25 $\mu$m, applies to all.

the A$\beta$40 staining remained stable, but the Congo red staining increased.

Even as early as the 6-month time point, A$\beta$ deposits were invested with dystrophic neurites. Both APP immunostaining (Figs. 4A and 4B) and synaptophysin immunostaining (Figs. 4D and 4E) decorated neurites around congophilic deposits in both gray matter (Figs. 4A and 4D) and white matter (Figs. 4B and 4E). Neurites surrounding amyloid deposits were also stained with antibody SMI-312 against phosphorylated neurofilament (Fig. 4C) and positively labeled with a silver stain (Fig. 4F). The early deposits were also stained with thioflavin S, further confirming their fibrillar nature (Fig. 4G). Unlike these other markers, only a subset of deposits at 6 months were stained with antiserum for ubiquitin (Fig. 4H); however, the proportion of ubiquitin-positive deposits increased as the mice aged. Finally, there are some antisera which fail to stain the neurites around plaques, such as that for the heparan sulfate proteoglycan, perlecan (Fig. 4I).

Astrocyte reactivity to the amyloid deposits was measured anatomically with GFAP immunostaining. At 3 months of age, GFAP immunostaining was largely

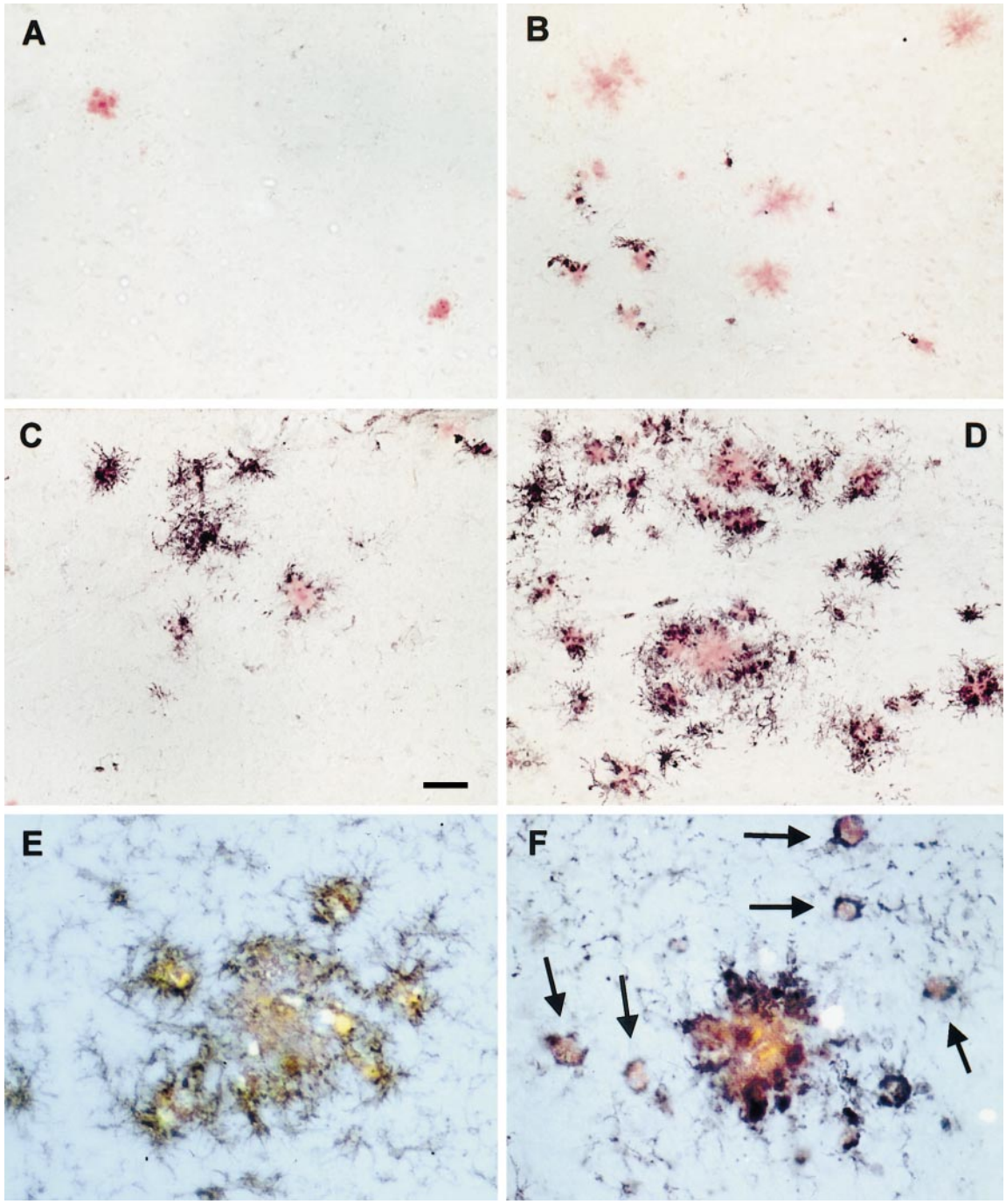


**FIG. 7.** Microglial activation in doubly transgenic mice. Sections were immunostained for MHC-II antigen from mice at 6 (A), 9 (B), 12 (C), or 15 months (D). In addition, sections from 12-month-old mice were stained with antibodies to complement receptor-3 (CD-11; mac-1 antibody; E) or antibody F4/80 (F). Scale bar, 100 $\mu$m in A–D, 12 $\mu$m in E, and 18 $\mu$m in F.

restricted to the hippocampus and white matter tracts such as corpus callosum. The frontal cortex in particular was free of GFAP-stained material, except for an occasional blood vessel and the glial limitans. At 6 months of age, the scattered amyloid deposits were surrounded by a cluster of activated astrocytes stained with GFAP, appearing as small patches in Fig. 5B. However, within these patches the activation of astrocytes could be considerable, with thickened, darkly stained processes (Fig. 5G). At 11 (Fig. 5C) and 15 months (Fig. 5D) the intensity of the GFAP immunostaining increased in most brain areas. In part, this was due to an increased number of deposits and a subsequent decline in the amount of neuropil without

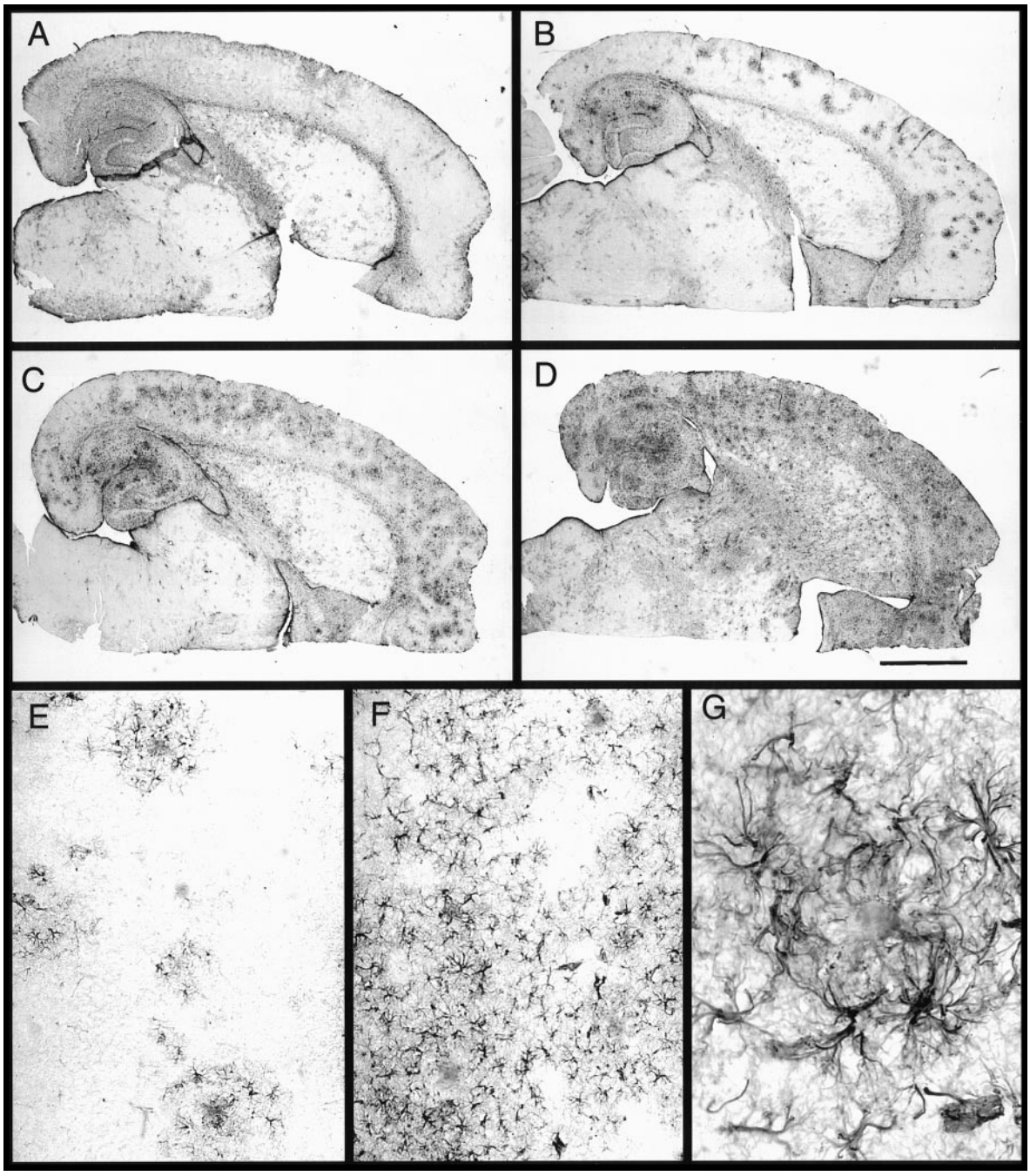


**FIG. 5.** Time course of GFAP immunostaining in doubly transgenic mice. Horizontal sections were stained for GFAP at 3 (A), 6 (B, E, G), 11 (C, F), and 17 months (D). Scale bar, 1 mm in A–D, 100 $\mu$m in E and F, and 25 $\mu$m in G.

reactive astrocytes (Figs. 5E and 5F). By 15 months there was also increased astrocyte staining in striatum and the clusters of reactive astrocytes in the cerebral cortex became confluent.

Neurochemical measurement of GFAP by ELISA confirmed this general time course (Fig. 6). Compared with nontransgenic mice, increased GFAP was found in the neocortex + hippocampus dissection of doubly transgenic mice at the 10.5- and 15-month time points. It is likely this is due to the presence of amyloid in the transgenic animals, as there was no effect of genotype on the GFAP content of the basal forebrain + brain stem dissections. This general time course paralleled the measurements of GFAP load in immunostained sections, with substantial increases at 11.5 and 17 months of age (Fig. 6A). Compared to other genotypes, the GFAP content in the doubly transgenic mice greatly exceeded that in the PS1 or APP mice at 15 months of age (Fig. 6B).

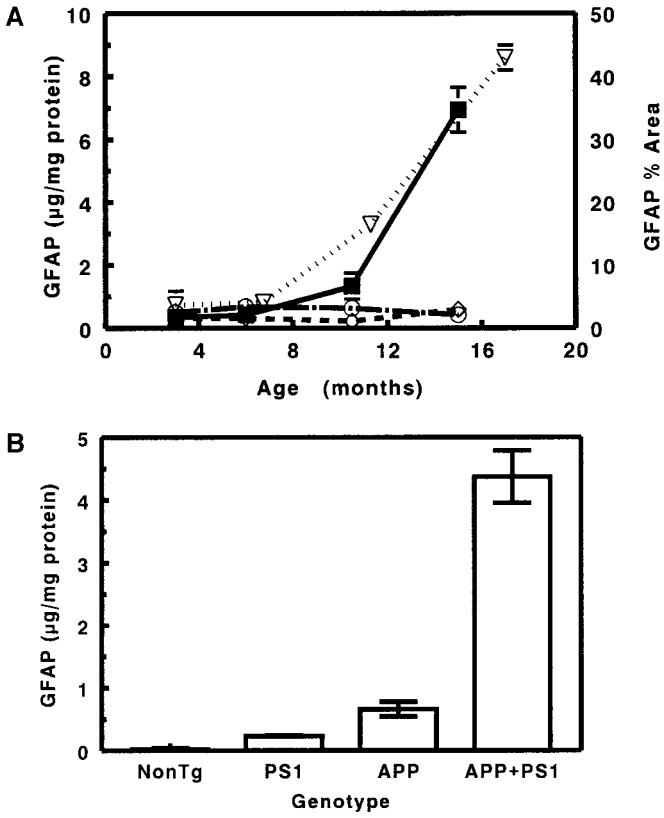


**FIG. 6.** GFAP increases over time in doubly transgenic mouse brain. In panel A, horizontal sections were stained with antiserum for GFAP and the reaction product area was quantified in frontal cortex (open triangles). In different mice, ELISA measurements of GFAP were made on the hippocampus plus cortex dissection from APP+PS1 transgenic mice (solid squares), the basal forebrain plus brain-stem dissection from APP+PS1 transgenic mice (diamonds), or the cortex plus hippocampus from nontransgenic mice (circles). The *n* for each group was as in Fig 3. Data presented are means ± SEM. In some cases the standard error was less than the diameter of the symbol. In panel B, the four genotypes of mice are compared at 16 months of age. The sample size per group is 11 for the nontransgenic (NonTg) and PS1 groups, 10 for the APP+PS1 group, and 8 for the APP group.

Activation of microglia was also evident in these mice. At 6 months of age, despite the presence of congophilic deposits, we have yet to observe an MHC-II-immunopositive microglial cell (Fig. 7A). At 9 months of age, we found, on rare occasions, some immunopositive microglia in association with congophilic deposits (Fig. 7B). By 12 months of age, MHC-II-stained microglia were found in a majority of the mice, with most of the microglia in intimate association with congophilic deposits (Fig. 7C). By 16 months of age, virtually all of the doubly transgenic mice had MHC-II-stained microglia, and not all were in apparent association with deposits (Fig. 7D). Nonetheless, there was considerable variability in the numbers of MHC-II-stained cells, which was not correlated with the amount of amyloid in each mouse, and occasional mice had very few MHC-II-stained cells. Measurement of immunopositive areas showed a late increase in MHC-II-staining of microglia beginning between 10 and 12 months of age (Fig. 8) and increasing dramatically over the next several months. We emphasize there was considerable inter-animal variability (note the large error bars at 16- and 18-month time points).

Activated microglia could also be detected using other markers. Complement receptor-3 immunostaining (CR3, CD11, mac-1) labeled microglia in association with amyloid deposits as early as 6 months (not shown). By 12 months, CR3-stained processes could be observed surrounding small amounts of congophilic material in the vicinity of larger deposits (Fig. 7E). Another microglia marker, antibody F4/80, produced a similar profile, with some instances in which the congophilic material was apparently circumscribed by the cytoplasm of a single microglial cell (arrows; Fig. 7F).

At the 16-month time point, all forms of AD-like pathology were more pronounced in the doubly transgenic mice than in the other three genotypes born in each litter. With regard to the measures of amyloid deposition, the mPS1 mice failed to deposit, with values equal to those of nontransgenic mice for $A\beta_{TOT}$ immunostaining (Fig. 9A) and Congo red staining (Fig. 9B). All APP-only mice exhibited amyloid deposits by this age, but the quantity of deposits in the PS1+APP doubly transgenic mice was three to fourfold greater than the APP-only mice (Figs. 9A and 9B). Regarding the presence of microglia, the doubly transgenic mice again had greater staining. For the CR3 marker, this was roughly a twofold elevation over the level of the other genotype groups. It should be noted that there was considerable basal expression of the CR3 marker in microglia. However,

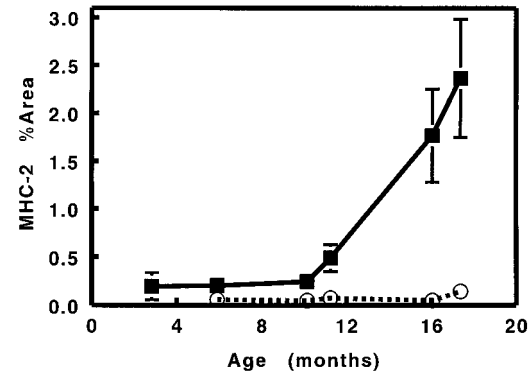


**FIG. 8.** MHC-II immunostaining increases with age in doubly transgenic mice. The reaction product area for MHC-II in frontal cortex is shown for doubly transgenic mice (solid squares) or nontransgenic mice (open circles). The sample size for each group was 3 at 3 months of age, 9 at 6 months, 5 at 10 months, 4 at 11 months, 10 at 16 months, and 4 at 18 months. Data presented are means ± SEM. In some cases the standard error was less than the diameter of the symbol.

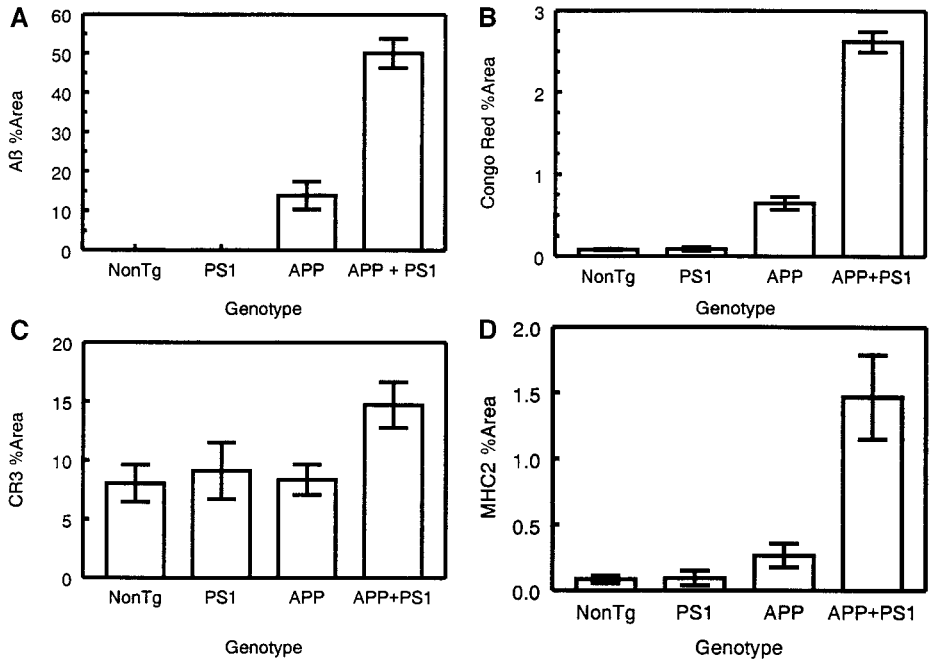


**FIG. 9.** Effects of genotype on amyloid deposits and microglial staining in 16-month-old mice. The reaction product areas for $A\beta_{TOT}$ (A), Congo red staining (B), complement receptor-3 immunostaining (C), and MHC-II immunostaining (D) are presented for the four genotype groups used in these studies. Data are from 11–22 nontransgenic, 6–18 PS1, 8–17 APP, and 10–23 APP+PS1 mice for each marker. Data presented are means ± SEM.

the clearest differences were found in the MHC-II immunostaining, for which the immunoreaction product area in the doubly transgenic mice was fivefold greater than that in the APP-only transgenics.

## DISCUSSION

As expected, both diffuse and fibrillar A$\beta$ deposits accumulate over the life span in doubly transgenic mice. In general, the pattern of deposition resembled that found in Alzheimer's disease. Compact deposits are largely restricted to cortex and hippocampus, with diffuse A$\beta$ deposits visible in other structures, including striatum (12). In these doubly transgenic mice, the diffuse deposits are primarily composed of A$\beta$42 while the compact deposits contain both C-terminal forms of the peptide, and the vascular A$\beta$ is primarily composed of A$\beta$40. This is virtually identical to the distributions of these C-terminal A$\beta$ variants in AD (21, 38).

Some other characteristics are unlike Alzheimer disease. Within the limits of measurement in this study, the initial histologically identifiable deposits are generally compact and congophilic, implying they consist mostly of fibrillar A$\beta$. The diffuse deposits do not appear until later. This is opposite the general perception that in AD the compact deposits are formed by condensation of the diffuse material (28, 45), with the caveat that it is difficult to make dynamic interpretations of plaque progression from the static images obtained in postmortem cases. However, in Down's syndrome, in which virtually all individuals develop plaque and tangle pathology by 40, and many also develop a dementia syndrome, the deposits found in the youngest cases (some as early as 8 years) appear to be diffuse A$\beta$, lacking dystrophic neurites or glial activation (25, 33, 42).

These early deposits in transgenic mice are circumscribed by dystrophic neurites, expressing many of the markers associated with dystrophic neurites in AD (8). Importantly, neurites containing paired-helical filaments are absent in these mice as are neurofibrillary tangles (22).

GFAP reactivity is argued to be one of the most sensitive indices of neuronal toxicity (36). At young ages when the number of A$\beta$ deposits is low, GFAP-labeled cortical astrocytes are localized to the immediate vicinity of the A$\beta$ deposits. With age the reactive astrocytes become confluent, with increased reactivity measured even between 11 and 16 months. This increase in histologically detectable GFAP is mirrored by a similar elevation in GFAP levels in cortex + hippocampus detected by ELISA. Although GFAP is well recognized to increase with age in mouse brain (15, 37), this does not contribute substantially to the increase found in the transgenic mice, as increases in the nontransgenic littermates remain negligible (Figs. 6A and 6B). While the initial increase in GFAP staining appears due to the presence of compact amyloid deposits, the later substantial increases are likely caused by other factors, as the number of compact deposits is

relatively stable during this period. The increase in numbers of MHC-II-immunoreactive microglia suggests that an inflammatory process is beginning during this interval.

Like several other groups (5, 10, 29, 41), we find increased staining of microglia in the vicinity of deposits at early time points (6 months) using markers which also stain resting microglia (in our case complement receptor-3). However, when we stain for microglia using MHC-II antisera, the reactivity is negligible before 12 months of age, and even in 15-month-old mice it is quite variable, with some mice having few immunoreactive cells. This may be a critical step in recapitulating AD, as MHC-II is the murine equivalent of the HLA-DR antigen found extensively upregulated in microglia from demented patients. Indeed, cases referred to as high-plaque normals (autopsy brains with high amyloid loads but no indications of dementia) generally do not stain for HLA-DR (26). Age may be a significant predisposing factor for the MHC-II increases reported here. In rats lesioned with 6-hydroxydopamine, we found that enhanced staining of striatal microglia with MHC-II was not evident until midlife and was even greater in older rats (32). It might be expected that transgenic mice age 20 months or older might all have considerable MHC-II activation. It is also interesting that a study of Tg 2576 mice (the APP contribution to the APP+PS1 mice used here) found increased IL-1 expression in 14-month-old mice, but not in 12- or 13-month-old animals (30).

From our work on behavioral changes in these doubly transgenic mice, we know that learning and memory deficits develop between 12 and 15 months (2, 31). Moreover, these deficits found in 15-month-old mice are correlated with the abundance of compact A$\beta$ deposits in their frontal cortices (13). From the present work, it is evident that glial cells increase their reactivity during this time. Microglia begin expressing MHC-II, and astrocytes dramatically upregulate GFAP expression. Although we would like to speculate that the MHC-II activation might be associated with a more severe state of neural inflammation that causes memory dysfunction, we have not been able to correlate memory performance with MHC-II staining in several different studies, all of which did detect correlations of memory performance with plaque loads (2, 13, 31).

Future studies will evaluate the role of MHC-II-bearing microglia in the potential removal of A$\beta$ deposits. This was first suggested in transgenic mice by the work with A$\beta$ vaccination, which found that the vaccine caused MHC-II expression in microglia and reductions in A$\beta$ deposits (39). We similarly find that the vaccine approach upregulates MHC-II expression (D. Wilcock, D. Morgan, and M. Gordon, in preparation) and that LPS injection into doubly transgenic mice activates microglia and reduces amyloid load (G. DiCarlo *et al.*, submitted for publication). The coincidence of MHC-II activation and the apparent stabilization of compact A$\beta$ deposition at 12 months of age found here is consistent with the hypothesis that activated microglia might be engulfing and clearing amyloid deposits. Biopsy studies from early AD patients that are followed to autopsy report little change in plaque densities during the disease course (4, 27). It has been suggested that amyloid plaques turn over in AD brain, achieving a steady state during the disease (20). In other work we find that a novel anti-inflammatory drug which dramatically reduces A$\beta$ loads also causes a paradoxical increase in the numbers of MHC-II-stained microglia (see Ref. 23 for a preliminary report). Together, these data suggest that microglial activation may have a dual action; some degree and/or types of activation may facilitate the clearance of A$\beta$ deposits. However, excessive activation or the type associated with inflammation will lead to the neurodestructive events so well characterized in Alzheimer disease (1).

## ACKNOWLEDGMENTS

This work was supported by AG 15490 (M.N.G.), AG 18478 (D.M.), and the Benjamin Alzheimer trust (D.M.). We thank Karen Hsiao-Ashe for providing the APP mice and Karen Duff for providing the PS1 mice and Paul Gottschall for the $A\beta_{TOT}$ antiserum.

## REFERENCES

1. Akiyama, H., S. Barger, S. Barnum, B. Bradt, J. Bauer, G. M. Cole, N. R. Cooper, P. Eikelenboom, M. Emmerling, B. L. Fiebich, C. E. Finch, S. Frautschy, W. S. Griffin, H. Hampel, M. Hull, G. Landreth, L. Lue, R. Mrak, I. R. Mackenzie, P. L. McGeer, M. K. O'Banion, J. Pachter, G. Pasinetti, C. Plata-Salaman, J. Rogers, R. Rydel, Y. Shen, W. Streit, R. Strohmeyer, I. Tooyoma, F. L. Van Muiswinkel, R. Veerhuis, D. Walker, S. Webster, B. Wegrzyniak, G. Wenk, and T. Wyss-Coray. 2000. Inflammation and Alzheimer's disease. *Neurobiol. Aging* **21:** 383–421.
2. Arendash, G. W., D. L. King, M. N. Gordon, D. Morgan, J. M. Hatcher, C. E. Hope, and D. M. Diamond. 2001. Progressive behavioral impairments in transgenic mice carrying both mutant APP and PS1 transgenes. *Brain Res.* **891:** 45–53.
3. Barrow, P. A., R. M. Empson, S. J. Gladwell, C. M. Anderson, R. Killick, X. Yu, J. G. Jefferys, and K. Duff. 2000. Functional phenotype in transgenic mice expressing mutant human presenilin-1. *Neurobiol. Dis.* **7:** 119–126.
4. Bennett, D. A., E. J. Cochran, C. B. Saper, J. B. Leverenz, D. W. Gilley, and R. S. Wilson. 1993. Pathological changes in frontal cortex from biopsy to autopsy in Alzheimer's disease. *Neurobiol. Aging* **14:** 589–596.
5. Benzing, W. C., J. R. Wujek, E. K. Ward, D. Schaffer, K. H. Ashe, S. G. Younkin, and K. R. Brunden. 1999. Evidence for glial-mediated inflammation in APPsw transgenic mice. *Neurobiol. Aging* **20:** 581–590.
6. Borchelt, D. R., T. Ratovitski, J. Van Lare, M. K. Lee, V. Gonzales, N. A. Jenkins, N. G. Copeland, D. L. Price, and S. S. Sisodia. 1997. Accelerated amyloid deposition in the brains of transgenic mice coexpressing mutant presenilin 1 and amyloid precursor protein. *Neuron* **19:** 939–945.

7. Borchelt, D. R., G. Thinakaran, C. B. Eckman, M. K. Lee, F. Davenport, T. Ratovitsky, C. M. Prada, G. Kim, S. Seekins, D. Yager, H. H. Slunt, R. Wang, M. Seeger, A. I. Levey, S. E. Gandy, N. G. Copeland, N. A. Jenkins, D. L. Price, S. G. Younkin, and S. S. Sisodia. 1996. Familial Alzheimer's disease-linked presenilin 1 variants elevate Abeta1-42/1-40 ratio in vitro and in vivo. *Neuron* **17:** 1005–1013.
8. Dickson, D. W. 1997. The pathogenesis of senile plaques. *J. Neuropathol. Exp. Neurol.* **56:** 321–339.
9. Duff, K., C. Eckman, C. Zehr, X. Yu, C. M. Prada, J. Perez-tur, M. Hutton, L. Buee, Y. Harigaya, D. Yager, D. Morgan, M. N. Gordon, L. Holcomb, L. Refolo, B. Zenk, J. Hardy, and S. Younkin. 1996. Increased amyloid-beta42(43) in brains of mice expressing mutant presenilin 1. *Nature* **383:** 710–713.
10. Frautschy, S. A., F. Yang, M. Irrizarry, B. Hyman, T. C. Saido, K. Hsiao, and G. M. Cole. 1998. Microglial response to amyloid plaques in APPsw transgenic mice. *Am. J. Pathol.* **152:** 307–317.
11. Games, D., D. Adams, R. Alessandrini, R. Barbour, P. Berthelette, C. Blackwell, T. Carr, J. Clemens, T. Donaldson, and F. Gillespie. 1995. Alzheimer-type neuropathology in transgenic mice overexpressing V717F beta-amyloid precursor protein. *Nature* **373:** 523–527.
12. Gearing, M., R. W. Wilson, E. R. Unger, E. R. Shelton, H. W. Chan, C. L. Masters, K. Beyreuther, and S. S. Mirra. 1993. Amyloid precursor protein (APP) in the striatum in Alzheimer's disease: An immunohistochemical study. *J. Neuropathol. Exp. Neurol.* **52:** 22–30.
13. Gordon, M. N., D. L. King, D. M. Diamond, P. T. Jantzen, K. L. Boyett, C. E. Hope, J. M. Hatcher, G. DiCarlo, P. Gottschal, D. Morgan, and G. W. Arendash. 2001. Correlation between cognitive deficits and A$\beta$ deposits in transgenic APP+PS1 mice. *Neurobiol. Aging* **22:** 377–385
14. Gordon, M. N., W. A. Schreier, X. Ou, L. A. Holcomb, and D. G. Morgan. 1997. Exaggerated astrocyte reactivity after nigrostriatal deafferentation in the aged rat. *J. Comp Neurol.* **388:** 106–119.
15. Goss, J. R., C. E. Finch, and D. G. Morgan. 1991. Age-related changes in glial fibrillary acidic protein RNA in the mouse brain. *Neurobiol. Aging* **12:** 165–170.
16. Holcomb, L., M. N. Gordon, E. McGowan, X. Yu, S. Benkovic, P. Jantzen, K. Wright, I. Saad, R. Mueller, D. Morgan, S. Sanders, C. Zehr, K. O'Campo, J. Hardy, C. M. Prada, C. Eckman, S. Younkin, K. Hsiao, and K. Duff. 1998. Accelerated Alzheimer-type phenotype in transgenic mice carrying both mutant amyloid precursor protein and presenilin 1 transgenes. *Nat. Med.* **4:** 97–100.
17. Holcomb, L. A., M. N. Gordon, P. Jantzen, K. Hsiao, K. Duff, and D. Morgan. 1999. Behavioral changes in transgenic mice expressing both amyloid precursor protein and presenilin-1 mutations: Lack of association with amyloid deposits. *Behav. Genet.* **29:** 177–185.
18. Holcomb, L. A., M. N. Gordon, E. McGowan, X. Yu, S. Benkovic, P. Jantzen, K. Wright, I. Saad, R. Mueller, D. Morgan, S. Sanders, C. Zehr, K. O'Campo, J. Hardy, C. M. Prada, C. Eckman, S. Younkin, K. Hsiao, and K. Duff. 1998. Accelerated Alzheimer-type phenotype in transgenic mice carrying both mutant amyloid precursor protein and presenilin 1 transgenes. *Nat. Med.* **4:** 97–100.
19. Hsiao, K., P. Chapman, S. Nilsen, C. Eckman, Y. Harigaya, S. Younkin, F. Yang, and G. Cole. 1996. Correlative memory deficits, Abeta elevation, and amyloid plaques in transgenic mice. *Science* **274:** 99–102.
20. Hyman, B. T., K. Marzloff, and P. V. Arriagada. 1993. The lack of accumulation of senile plaques or amyloid burden in Alzheimer's disease suggests a dynamic balance between amyloid deposition and resolution. *J. Neuropathol. Exp. Neurol.* **52:** 594–600.
21. Iwatsubo, T., A. Odaka, N. Suzuki, H. Mizusawa, N. Nukina, and Y. Ihara. 1994. Visualization of A$\beta$42(43) and A$\beta$40 in senile plaques with end-specific A$\beta$ monoclonals: Evidence that an initially deposited species is A$\beta$42(43). *Neuron* **13:** 45–53.
22. Jaffar, S., S. E. Counts, S. Y. Ma, E. Dadko, M. N. Gordon, D. Morgan, and E. J. Mufson. Neuropathologic alterations in mutant APPswe and PS1m1461 and doubly transgenic mice: A selective increase in p75ntr-containing basal forebrain neurons. Submitted for publication.
23. Jantzen, P. T., M. N. Gordon, K. Connor, G. DiCarlo, and D. Morgan. 2000. Modification of microglial reactivity in mAPP/mPS1 transgenic mice using NCX-2216. *Neurosci. Abstr.* **30:** 379.8.
24. Johnson-Wood, K., M. Lee, R. Motter, K. Hu, G. Gordon, R. Barbour, K. Khan, M. Gordon, H. Tan, D. Games, I. Lieberburg, D. Schenk, P. Seubert, and L. McConlogue. 1997. Amyloid precursor protein processing and A beta42 deposition in a transgenic mouse model of Alzheimer disease. *Proc. Nat. Acad. Sci. USA* **94:** 1550–1555.
25. Leverenz, J. B., and M. A. Raskind. 1998. Early amyloid deposition in the medial temporal lobe of young Down syndrome patients: A regional quantitative analysis. *Exp. Neurol.* **150:** 296–304.
26. Lue, L., L. Brachova, H. Civin, and J. Rogers. 1996. Inflammation, Abeta deposition and neurofibrillary tangle formation as correlates of Alzheimer's disease neurodegeneration. *J. Neuropathol. Exp. Neurol.* **55:** 1083–1088.
27. Mann, D. M., B. Marcyniuk, P. O. Yates, D. Neary, and J. S. Snowden. 1988. The progression of the pathological changes of Alzheimer's disease in frontal and temporal neocortex examined both at biopsy and at autopsy. *Neuropathol. Appl. Neurobiol.* **14:** 177–195.
28. Mann, D. M. A. 1989. The pathogenesis and progression of the pathological changes of Alzheimer's disease. *Ann. Med.* **21:** 133–136.
29. McGowan, E., S. Sanders, T. Iwatsubo, A. Takeuchi, T. Saido, C. Zehr, X. Yu, S. Uljon, R. Wang, D. Mann, D. Dickson, and K. Duff. 1999. Amyloid phenotype characterization of transgenic mice overexpressing both mutant amyloid precursor protein and mutant presenilin 1 transgenes. *Neurobiol. Dis.* **6:** 231–244.
30. Mehlhorn, G., M. Hollborn, and R. Schliebs. 2000. Induction of cytokines in glial cells surrounding cortical beta-amyloid plaques in transgenic Tg2576 mice with Alzheimer pathology. *Int. J. Dev. Neurosci.* **18:** 423–431.
31. Morgan, D., D. M. Diamond, P. E. Gottschall, K. E. Ugen, C. Dickey, J. Hardy, K. Duff, P. Jantzen, G. DiCarlo, D. Wilcock, K. Connor, J. Hatcher, C. Hope, M. Gordon, and G. W. Arendash. 2000. A beta peptide vaccination prevents memory loss in an animal model of Alzheimer's disease. *Nature* **408:** 982–985.
32. Morgan, D., and M. N. Gordon. 1996. Aging and molecular biology. Pages 468–487 in D. Magnusson, Ed., *The Lifespan Development of Individuals*. Cambridge Univ. Press, New York.
33. Motte, J., and R. S. Williams. 1989. Age-related changes in the density and morphology of plaques and neurofibrillary tangles in Down syndrome brain. *Acta Neuropathol.* **77:** 535–546.
34. Mucke, L., E. Masliah, G. Q. Yu, M. Mallory, E. M. Rockenstein, G. Tatsuno, K. Hu, D. Kholodenko, K. Johnson-Wood, and L. McConlogue. 2000. High-level neuronal expression of Abeta 1–42 in wild-type human amyloid protein precursor transgenic mice: Synaptotoxicity without plaque formation. *J. Neurosci.* **20:** 4050–4058.

35. O'Callaghan, J. P. 1991. Quantification of glial fibrillary acidic protein: Comparison of slot-immunobinding assays with a novel sandwich ELISA. *Neurotoxicol. Teratol.* **13:** 275–281.

36. O'Callaghan, J. P., and K. F. Jensen. 1992. Enhanced expression of glial fibrillary acidic protein and the cupric silver degeneration reaction can be used as sensitive and early indicators of neurotoxicity. *Neurotoxicology* **13:** 113–122.

37. O'Callaghan, J. P., and D. B. Miller. 1991. The concentration of glial fibrillary acidic protein increases with age in the mouse and rat brain. *Neurobiol. Aging* **12:** 171–174.

38. Savage, M., J. Kawooya, L. Pinsker, T. Emmons, S. Mistretta, R. Siman, and B. Greenberg. 1995. Elevated A$\beta$ levels in Alzheimer's disease brain are associated with a selective accumulation of A$\beta$42 in parenchymal amyloid deposits, and both A$\beta$40 and A$\beta$42 in cerebrovascular deposits. *Amyloid Int. J. Exp. Clin. Invest.* **2:** 234–240.

39. Schenk, D., R. Barbour, W. Dunn, G. Gordon, H. Grajeda, T. Guido, K. Hu, J. Huang, K. Johnson-Wood, K. Khan, D. Kholodenko, M. Lee, Z. Liao, I. Lieberburg, R. Motter, L. Mutter, F. Soriano, G. Shopp, N. Vasquez, C. Vandevert, S. Walker, M. Wogulis, T. Yednock, D. Games, and P. Seubert. 1999. Immunization with amyloid-beta attenuates Alzheimer-disease-like pathology in the PDAPP mouse. *Nature* **400:** 173–177.

40. Smith, J. K., R. I. Krohn, G. T. Hermanson, A. K. Mallia, F. H. Gartner, M. D. Provenzano, E. K. Fujimoto, N. M. Goeke, B. J. Olson, and D. C. Klenk. 1985. Measurement of protein using bicinchoninic acid. *Anal. Biochem.* **150:** 76–85.

41. Stalder, M., A. Phinney, A. Probst, B. Sommer, M. Staufenbiel, and M. Jucker. 1999. Association of microglia with amyloid plaques in brains of APP23 transgenic mice. *Am. J. Pathol.* **154:** 1673–1684.

42. Stoltzner, S. E., T. J. Grenfell, C. Mori, K. E. Wisniewski, T. M. Wisniewski, D. J. Selkoe, and C. A. Lemere. 2000. Temporal accrual of complement proteins in amyloid plaques in Down's syndrome with Alzheimer's disease. *Am. J. Pathol.* **156:** 489–499.

43. Sturchler-Pierrat, C., D. Abramowski, M. Duke, K. H. Wiederhold, C. Mistl, S. Rothacher, B. Ledermann, K. Burki, P. Frey, P. A. Paganetti, C. Waridel, M. E. Calhoun, M. Jucker, A. Probst, M. Staufenbiel, and B. Sommer. 1997. Two amyloid precursor protein transgenic mouse models with Alzheimer disease-like pathology. *Proc. Natl. Acad. Sci. USA* **94:** 13287–13292.

44. Wengenack, T. M., G. L. Curran, and J. F. Poduslo. 2000. Targeting Alzheimer amyloid plaques in vivo. *Nat. Biotechnol.* **18:** 868–872.

45. Wisniewski, H. M., C. Bancher, M. Barchikowska, G. Y. Wen, and J. Currie. 1989. Spectrum of morphological appearance of amyloid deposits in Alzheimer's disease. *Acta Neuropathol.* **78:** 337–347.